

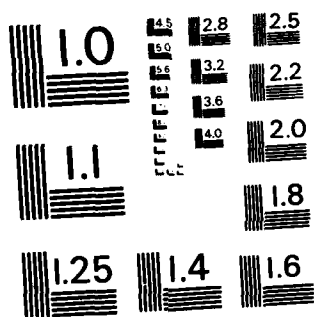
AD-A131 037 APPLICATIONS OF ION-BEAM MILLING AND DEPOSITION
TECHNIQUES TO MEL (HIGH E.) (U) NEW MEXICO STATE UNIV
LAS CRUCES PHYSICAL SCIENCE LAB J R MCNEIL 23 NOV 81
UNCLASSIFIED DAAH01-80-C-1220 F/G 20/7

APPLICATIONS OF ION-BEAM MILLING AND DEPOSITION
TECHNIQUES TO MEL (HIGH E.) (U) NEW MEXICO STATE UNIV
LAS CRUCES PHYSICAL SCIENCE LAB J R MCNEIL 23 NOV 81
DAAH01-80-C-1220 F/G 20/7

1/1

NL

END
DATE
FILMED
6 83
BT



MICROCOPY RESOLUTION TEST CHART
NATIONAL BUREAU OF STANDARDS - 1963-A

AD A131037

DTIC FILE COPY

Applications of Ion-Beam Milling and Deposition Techniques to HEL Optics

FINAL REPORT

Contract DAAH01-80-C-1220

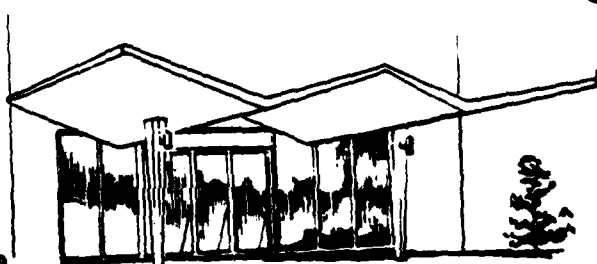
Submitted to

Army High Energy Laser Systems Program Office
Redstone Arsenal, Alabama

by

Dr. J. R. McNeil

23 November 1981



Physical Science Laboratory

Box 3-PSL, Las Cruces, New Mexico 88003
Area (505) 522-9100 TWX 910-983-0541

This document has been approved
for public release and its
distribution is unlimited.

83 07 29 032

ABSTRACT

This effort was a feasibility investigation to examine applications of ion beam techniques to optical substrates and dielectric coating material, to remove or add material to the surface of an optic in a controlled manner during fabrication. Removing material by ion beam milling is accomplished at the expense of increased surface roughness. Measurements of optical surface roughness were made versus milling depth for various ion beam conditions and geometry arrangements. A Twyman-Green interferometer was constructed such that the optical surface could be observed in the vacuum chamber during coating or ion milling. The accomplishments of this effort can be summarized as follows:

- (1) Cu does not appear satisfactory for being ion milled to improve surface figure.
- (2) Ion beam sputter deposition of Cu onto Cu substrates appears to reduce microroughness of the substrates.
- (3) The other materials examined -- Mo, Si, glasses, electroless Ni, ZnS, ZnSe, MgF_2 , and ThF_4 -- can be milled in a controlled manner. The amount that can be milled from the optic without severe increase in roughness depends upon the application. However, in general the increase in roughness for milling less than 0.5 fringe is less than the initial surface roughness of the optic.
- (4) The value of the interferometer for in-vacuum monitoring of optic surface figure has been demonstrated to:
 - A. Selectively deposit material on an optic and selectively ion beam mill an optical surface; repair a nonuniform optical surface.
 - B. Repeated deposit/mill/deposit optical material without breaking vacuum.
- (5) Ion beam sputter deposition of ZnS appears to produce films of good optical quality; deposition of ThF_4 using ion beam sputtering produces films of questionable absorbance. A hybrid technique for deposition of ZnS has been demonstrated that incorporates advantages of sputter deposition and thermal deposition. The sputter yield of ThF_4 is too

low in the present geometry to make the process viable. More detailed investigations of these films are needed.

Recommendations are given for future applications of ion beam techniques for deposition of dielectric materials.



copy sent on file
R83-1548

A

Table of Contents

	<u>Page No.</u>
Abstract.	i
1.0 INTRODUCTION	1
1.1 Review of High Energy Laser Optics Quality Requirements . .	1
1.1.1 Effect of Aberrations.	2
1.1.2 Metal Substrate Fabrication Limitations.	2
1.1.3 Dielectric Coating Limitations	5
1.1.4 Summary of HEL Optics Quality Requirements	8
1.2 Past Work	8
1.2.1 Ion Beam Milling	8
1.2.2 Sputter Deposition	9
1.3 Goals of this Effort.	10
2.0 EXPERIMENTAL ARRANGEMENT AND PROCEDURES.	11
3.0 RESULTS AND DISCUSSION	15
3.1 Selective Deposition and Milling to Improve the Figure of an Optic	15
3.2 Effect of Ion Beam Milling on Surface Roughness and Optical Transmission of Substrate and Dielectric Coating Materials. 18	18
3.2.1 Optical Substrate Materials.	18
3.2.2 Dielectric Coating Materials	25
3.2.3 Surface Roughness Dependence on Ion Beam Milling Parameters	30
3.3 Sputter Rates of Materials.	32
3.4 Effect of Ion Beam Sputter Deposition to Reduce Surface Roughness	34
3.5 Ion Beam Deposition of Dielectric Coating Materials	38
3.5.1 Sputter-Thermal Deposition Technique	38
3.5.2 Optical Properties of Ion Beam Sputtered ZnS and ThF	40
3.5.3 Future Possible Applications of Ion Beams to Thin Film Coating.	42
4.0 SUMMARY.	43
References.	44

List of Figures

	<u>Page No.</u>
Figure 1. Equivalent figure error in a MLD-Coated mirror caused by nonuniform film thickness across the mirror	6
Figure 2. Photographs of interference pattern produced using a Twyman-Green interferometer with one leg in the vacuum deposition chamber	14
Figure 3. Demonstration of selectively milling an optic to introduce a 1500 Å step and the repair of the optic by selectively milling the opposite side	16
Figure 4. Demonstration of selectively depositing material on an optic to introduce a 1500 Å step and the partial repair to the optic by selectively milling the same side.	17
Figure 5. Surface roughness, δ_{RMS} , resulting from ion beam milling Cu substrates, versus milling depth.	19
Figure 6. Surface roughness, δ_{RMS} , resulting from ion beam milling Mo substrates, versus milling depth.	21
Figure 7. Surface roughness, δ_{RMS} , resulting from ion beam milling Si substrates, versus milling depth	22
Figure 8. Surface roughness, δ_{RMS} , resulting from ion beam milling different glass-like materials substrates, versus milling depth	23
Figure 9. Surface roughness, δ_{RMS} , resulting from ion beam milling electroless Ni and Al substrates, versus milling depth.	24

List of Figures (Continued)

	<u>Page No.</u>
Figure 10. Surface roughness, δ_{RMS} , resulting from ion beam milling ZnS substrates, versus milling depth.	26
Figure 11. Surface roughness, δ_{RMS} , resulting from ion beam milling ZnSe substrates, versus milling depth.	27
Figure 12. Surface roughness, δ_{RMS} , resulting from ion beam milling MgF_4 substrates, versus milling depth.	28
Figure 13. Surface roughness, δ_{RMS} , resulting from ion beam milling MgF_2 substrates, versus milling depth.	29
Figure 14. Illustration of how energetic atoms, which become adatoms with high surface mobility, might tend to reduce micro-roughness of a surface.	37
Figure 15. Deposition rate observed (for the particular geometry employed) versus ion beam current for ion beam deposited	39
Figure 16. Spectrophotometer scans of ion beam deposited films.	41

List of Tables

	<u>Page No.</u>
Table 1: Summary of cost required to take the surface figure of Cu and Mo optics from $\lambda/1$ to $\lambda/10$	4
Table 2: Effects of ion beam milling on surface roughness for different experimental conditions.	31
Table 3: Summary of ion milling rates of the samples investigated	33
Table 4: Effect of Ion Beam Deposited Cu Films on Surface Roughness of Ion Beam Milled/Roughened Surfaces.	35

1.0 INTRODUCTION

This effort addressed the potential for applying ion beam techniques to different stages of optical component fabrication to remove material from or add material to the surface of an optic in a precise manner. In conjunction with this, a Twyman-Green interferometer was constructed to monitor the condition of the optical surface in situ. Realization of these techniques might allow an optic to be shaped, cleaned, coated, and examined during the different stages of fabrication without breaking vacuum. This would have advantages for improving component quality while making it possible to automate some phases of fabrication.

1.1 Review of High Energy Laser Optics Quality Requirements

Large diameter optics (3" to several meters) are required for many laser applications for several reasons. First, the laser resonator itself is often composed of large optics, some of which may be complex in shape. Second, the efficiency with which an optical system can focus laser output to a spot increases with increasing diameter of the optical beam and increasing diameter of the components of the optical system. This can easily be illustrated by considering the imaging of a system, where for simplicity the light intensity is uniform across the exit pupil of radius a . This is described in terms of a diffraction problem. Bennett¹ has discussed this situation and has shown that at a focal distance f from the optical system, the peak intensity at the target I_o is approximately

$$I_o = \left(\frac{\pi a^2 E}{\lambda f} \right)^2, \quad (1)$$

where λ and E are the wavelength and field strength, respectively, of the light. The output power of the laser can be expressed as $P = \pi a^2 E^2$, allowing I_o to be written as

$$I_o = \pi P (a/\lambda f)^2. \quad (2)$$

Thus, in the absence of aberrations the irradiance is directly proportional to the square of the exit pupil radius. This must naturally be modified when

considering a real light source which might not have a uniform intensity across the exit pupil. Third, the effects of thermal blooming are minimized with large diameter beams. These aspects are particularly important for systems in which it is desired to deposit as much of the laser output as possible on some relatively small area.

1.1.1 Effect of Aberrations

If aberrations or thermal blooming are present in the system, the peak intensity of the beam falls, even though the transmission or reflection characteristics of the optics do not appreciably reduce the total power of the beam. Bennett¹ and other investigators^{2,3} have analyzed this situation and find the peak intensity decreases nearly exponentially with the RMS wavefront distortion. Based on the Strehl criteria, the total amount of RMS distortion that will cause a 20% reduction in the value of I_0 given by equation (2) is approximately $\lambda/14$. This is a convenient design goal.

The discussion to this point illustrates the stringent requirements of optical substrate figure and coating uniformity that are required. This is particularly severe for multi-component systems. Error tolerances for individual optics must be established that take into account these two effects as well as thermal loading and other related causes of wavefront distortion. As an example, for a ten-component system operating at 3.8μ and considering only substrate figure and coating error, the optical figure for each element would have to be at least an eighth wave in the visible region. This assumes equal figure tolerance for each optic is allowable. This can be very difficult to achieve with metal optics and for large optics in general, particularly if they are to be coated with several layers of dielectric material.

1.1.2 Metal Substrate Fabrication Limitations

The materials more commonly used as reflector substrates for IR applications include Cu and Mo. Both materials are very difficult to machine and polish. One possible exception is with Mo that has been vacuum arc casted, has low carbon content, and has been appropriately treated to modify grain structure⁴. Unless Mo is treated in this proprietary manner, micro-cracks often appear

that make it difficult to achieve a good surface. Machining and polishing Cu is difficult because the material is so soft. To take the surface figure of a moderately large (e.g., 6") Cu flat from $\lambda/1$ to $\lambda/10$ is very difficult. Here λ is in the visible wavelength region. Similarly, for Mo optics this is rarely achieved⁴. Table 1 summarizes the approximate costs involved in extending the surface from $\lambda/1$ to $\lambda/10$ for different combinations of parameters. To obtain this price information several metal optical component vendors were contacted. Two claimed a $\lambda/10$ figure on a 1" diameter optic was not within their capability and suggested contacting SPAWR Optical Research, Inc. for the optics. SPAWR is the recognized leader in the manufacture of high quality metal optics, specializing in Cu. The information in Table 1 was quoted by SPAWR. Note that there is nearly a factor of 10 increase in price for small optics in taking a $\lambda/1$ surface to $\lambda/10$. For Cu optics larger than 6" diameter SPAWR was reluctant to quote. They have on occasion achieved a $\lambda/20$ surface on Cu optics.

One technique sometimes used to achieve a good surface figure on a large diameter optic is to make the overall diameter larger than required, and to use only a portion of the optic. However, for some applications this is not suitable. A scraper mirror in a high power laser cavity is an example. The optical figure must be of high quality up to the edge of the central hole of the optic. Achieving this causes the optic to be approximately four times as expensive as the optic having a good surface figure only to within approximately 1/8" of the central hole.

Diamond turning of metals has become popular in the last several years. This technique has an advantage over standard polishing techniques in that complex shapes can be produced with less effort than conventional methods. This is the only practical way to produce some complex surfaces.

Diamond turning, however, has drawbacks. At present it is difficult to achieve finishes that have less than 100 Å RMS surface variation^{4,5}, with several times this reported often for large Cu optics⁴. This is much greater than the values obtained for commercially available Cu optics that have been polished using conventional techniques and prohibits use of diamond-turned optics for some high power applications. Post-polishing techniques can be

Material	Diameter	Radius of Curvature	Surface figure ^{a)}	
			$\lambda/1$	$\lambda/10$
Cu	1"	∞	\$ 132	\$1,127
Cu	1"	5M	\$ 144	\$1,232 ^{b)}
Cu	6"	∞	\$ 688	\$2,588
Cu	6"	5M	\$ 722	\$2,632 ^{b)}
Mo	1"	∞	\$ 90	\$1,512
Mo	1"	5M	\$ 114	\$1,915 ^{b)}
Mo	6"	∞	\$1,320 ^{c)}	\$6,590 ^{c)}

a) λ is in visible.

b) Price does not include one-time test plate charge of approximately \$1,200.

c) Price does not includes surcharge of approximately \$1,100; this is variable and depends on Mo market.

Table 1: Summary of cost required to take the surface figure of Cu and Mo optics from $\lambda/1$ to $\lambda/10$. (Information from Reference 4).

employed to improve the situation for some shapes. However, this added step makes the process lose some of its appeal. Another objection to diamond turned optics concerns the diffraction grating effect caused by the machining lines left on the optical surface. The effect is more prevalent for small spacing between peaks on the surface. This can cause a loss of up to several percent.

Even if the desired optical quality and proper mounting are achieved, metal optics have a general tendency to creep without applied stress^{1,4}. There is thus the question of whether a large Cu mirror would retain a good optical figure over a period of time, even if it were initially satisfactory. Data in this area is sparse. However 12-inch diameter Mo mirrors have been examined¹. With a figure of $\lambda/8$ initially, after a period of three months this had deteriorated to $\lambda/2$ to $\lambda/4$ for several samples. Data is given for invar, Cer-Vit, ULE, and zerodur². Because of its soft nature, Cu optics tend to creep more and suffer from mounting distortion more than Mo optics⁴.

1.1.3 Dielectric Coating Limitations

Both substrate figure and coating uniformity must be considered when concerned about optical wavefront distortion. Bennett¹ has analyzed the effects of coating nonuniformity in light of the requirements described above. Figure 1 illustrates the equivalent figure error obtained as a function of film thickness error. Note first that the dashed line gives the figure error in visible wavelengths. Thus to achieve the eighth wave figure mentioned previously, a 2% tolerance in film thickness must be maintained. If thermal effects are considered, uniformity restrictions such as 1% or better are required. Second, note that both the axes in the figure scale with wavelength. So except for the position of the dashed line, the figure is relatively unchanged when considering other coating design wavelengths. Also note from Figure 1 that the reflectance changes very little for the range of film thickness error shown.

It should be emphasized that for many systems, multilayer dielectric coatings are desirable for use with metal optics. The stack can reduce the absorption appreciably, greater than an order of magnitude without elaborate designs

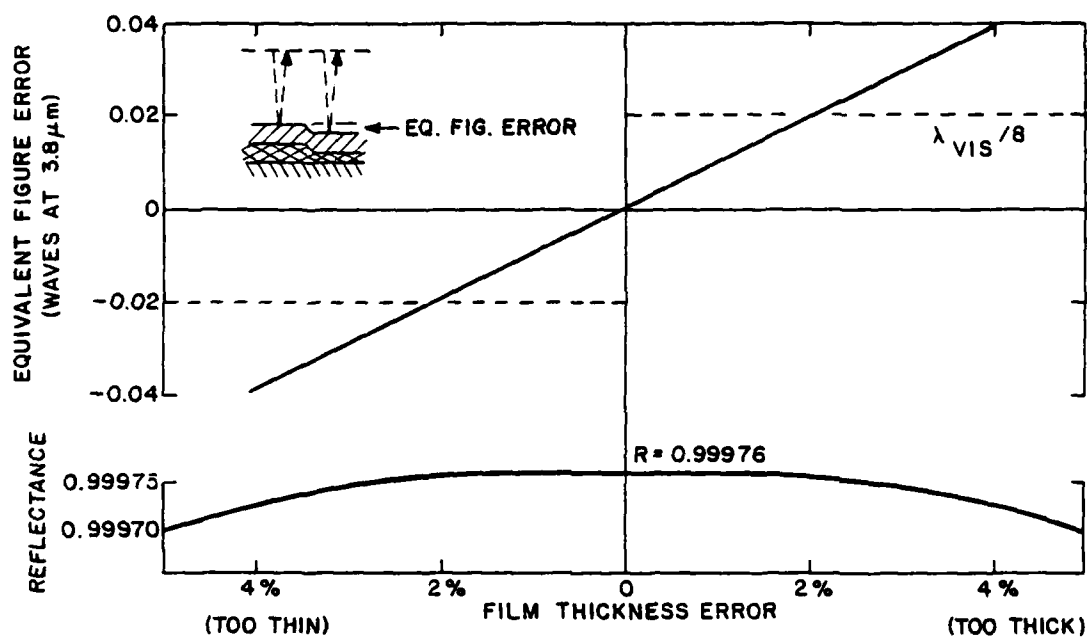


Figure 1. Equivalent figure error in a MLD-Coated mirror caused by nonuniform film thickness across the mirror. The multilayer coating design is $(\text{Zn}/\text{ThF}_4)^4 \text{ZnS}^x \text{Ag}$, and the design wavelength is 3.8μ . The dashed lines give the corresponding figure error in visible wavelengths. They would not be the observed figure errors if measurements were made in the visible, because of phase shift. (Figure from reference 1 with permission of H. E. Bennett).

required. This in turn reduces the error introduced by thermal effects and leaves more margin for other error. Therefore, there are tradeoff considerations involved when using multilayer stacks.

The effect of the requirements discussed above on the present optical fabrication technology is tremendous, particularly when considering large diameter (>1 meter) optics and large optics that must be coated. Bennett¹ has thoroughly discussed this impact and has reviewed several studies concerned with coating problems in particular. The magnitude of the problem can be realized by considering problems involved in coating a large optic. Most dielectrics are deposited from sources which can be approximated as a Lambertian source. For a geometry where the optical substrate is parallel to the source plane with a distance h between the planes, the thickness of the film deposited is given by

$$t = \frac{m}{\pi \rho} \frac{\cos^4 \theta}{h^2}, \quad (3)$$

where m is the total mass of the material emitted, ρ is the mass of the deposited film of thickness t , and θ is the angle between a line joining the source and a point on the optic and the line perpendicular to the source plane. From this expression the requirements of the coating system can be determined. As an example, to achieve a 1% uniform thickness film on a 4-meter-diameter mirror, the value of h would have to be 28 meters; because h would be so large, to avoid collisions between evaporant atoms and residual gas atoms, the chamber pressure would need to be $\sim 10^{-7}$ Torr.

Several steps could be taken to simplify the requirements. Stationary or moving masks could be employed to help compensate for the $\cos^4 \theta$ variation. Mask design has traditionally been accomplished on an empirical basis⁴. This can be tedious and expensive for large systems. Substrates can be rotated, and this helps the situation. Double-planetary rotation is not acceptable for large optics because of the increased chamber size that would be required. Offsetting the source from directly beneath the center of the optic improves the situation somewhat when masks are used.

In addition to the complexities described above, practical problems exist. Source emission is often not strictly as described by equation (3), and with

source usage the characteristics of emission change. Pressure-dependent variations can be significant when using an added gas at a pressure in the 10^{-4} Torr range. The gauging used to regulate pressure is often not extremely precise. The presence of the chamber wall can influence deposition rate for regions of the optic nearby. Optical and mechanical qualities of the optic are sensitive to the angle of incidence the evaporant makes with the optic.

1.1.4 Summary of HEL Optics Quality Requirements

Summarizing from the discussion above, the following points can be made concerning quality requirements of HEL optics:

- o For many HEL requirements, optics are required to have a figure that is either difficult to achieve now or is not within the limits of present technology.
- o To achieve a figure better than $\lambda_{vis}/1$ with low RMS roughness on metal optics is difficult and expensive.
- o The surface figure of metal optics degrades with time due to creep, mounting, and handling.
- o Coating large optics uniformly will be expensive and tedious, requiring large specialized facilities.

1.2 Past Work

1.2.1 Ion Beam Milling

Ion milling (polishing) of metal laser substrates prior to coating has been used in the past^{7,8} to demonstrate the advantages of the technique in producing coatings of superior adherence, reduced impurities at the film/substrate interface and coatings of lower absorptivity. The investigations described in References 7 and 8 involved application of ion beam technology prior to coating to prepare the substrate. First, single-crystal copper substrates were ion polished prior to being coated. In the second case, in situ deposition of the coatings was employed with favorable results. The ion beam source employed for this work produced beams with energies typically of 4 keV. Texturing was observed when polycrystalline copper substrates were ion polished, presumably due to differential sputtering of the crystallites of different orientations.

Ion beam milling has also been considered for shaping optical surfaces from fused silica, ULE and Cer-Vit^{9,10}. Surfaces were reported to have a roughness comparable to those of the same material produced by standard polishing techniques. This was in spite of the limited range of operation parameters of the ion beam source. Beam energies of ~ 50 keV were employed. Smoother surfaces were predicted from the use of a beam of less energetic ions⁹. Another drawback of the ion beam source used in the work of Reference 9 was the low ion flux supplied (~ 300 μ A). This directly effects the time required for working the optical components. The ion flux of the source used in this work was over 100 mA.

In none of the investigations of ion milling described above was there a detailed description given of the surface roughness effects and the variation of roughness with milling depth. Also, investigations have been performed primarily with high energy beams (>4 keV) at low total beam current. Sputtering rates depend drastically on incident particle energy for energies below several keV, as well as on incident angle^{13,14}. Also, to the author's knowledge there has been no investigation of milling dielectric materials commonly used in optical coating.

1.2.2 Sputter Deposition

Sputtered films have been investigated for a number of years for many applications. However, relatively little work has been done using ion beams to sputter deposit thin films for optical applications. Most sputter work has involved diode or triode arrangements excited by application of either dc or rf power, and in many cases the gas discharge, sputter target, and optical substrate are located such that the geometry is not very flexible.

Sputter deposition of optical materials has yielded films of very high quality for laser and other electro-optical applications^{15,16,17,18}. This is most likely attributable to the relatively high kinetic energy (1-10eV) of sputtered particles compared to particles emitted from an evaporation source of some type ($E \sim 0.1$ eV). This flux of high energy particles has several effects on film characteristics. First, a high surface temperature is produced without requiring bulk substrate heating, and this enhances surface mobility, diffusion,

chemical reactions, etc. Thus, a surface can be sputtered clean and kept clean during deposition while the film is forming. Interfacial structure - coating/substrate and coating/coating - is more intimate than in thermal deposition. A second effect of high energy particle arrival at the substrate is the production of films with higher packing density than those produced by other coating techniques. Higher packing density results in less absorption of impurities, such as water vapor. ZnS, ThF₄, cryolite and other film materials are prone to absorbing water vapor. In addition to causing the value for the index of refraction to be ambiguous, the absorbed materials cause lower damage thresholds at some wavelengths resulting from optical absorption. To the author's knowledge there has been no reported investigation of the optical properties of sputter-deposited fluorides (e.g., ThF₄) prepared using ion beams or other sputtering apparatus. These materials are commonly used in the visible and IR regions and are being investigated for applications in the ultraviolet.

1.3 Goals of this Effort

This effort was a feasibility investigation to examine application of ion beam techniques to optical substrates and dielectric coating material. A Twyman-Green interferometer was constructed such that the optical surface could be observed in the vacuum chamber during coating or ion milling. The primary goals of the effort included the following:

- Demonstrate the use and value of an interferometer for in-situ monitoring of optical surface figure to selectively deposit material on an optic and to selectively ion beam mill an optical surface; attempt to smooth a nonuniform optical surface to improve surface figure.
- Determine the effects of ion beam milling on the surface roughness of optical substrate materials (Cu, Mo, Si, fused silica, BK-7).
- Determine the effects of ion beam milling on the surface roughness of dielectric coating materials (ThF₄, MgF₂, ZnS, ZnSe).
- Determine the effects of ion beam sputter deposition to reduce surface roughness.
- Determine the optical characteristics of ion beam sputter-deposited dielectric coating materials (ThF₄, MgF₂, ZnS, and ZnSe).

As with any experimental program that is initiated, time and effort is spent in setup of basic laboratory apparatus.

2.0 EXPERIMENTAL ARRANGEMENT AND PROCEDURES

The following is a description of the equipment used for this effort:

Vacuum System. The system was a stainless steel 36" diameter bell jar and baseplate, pumped by a 6" diffusion pump with a cold trap. Base pressure was between 5×10^{-7} and 1×10^{-6} Torr, depending on system cleanliness. The system was fitted with a 5" tall instrumentation collar. This contained two 3" diameter ports used to pass the laser beam into the deposition chamber. Also, a number (12-14) O-ring-sealed feedthrus were used to manipulate shutters, substrate rotation and position, etc. Electrical and water feedthrus entered through the baseplate. The entire pump stand was vibration isolated from the floor. Mechanical pumps were vibration isolated from the pump stand.

Ion Source. The ion source was an Ion Tech 1" diameter beam Kaufman-type source. Total beam current possible exceeded 120 mA; beam voltage was adjustable between 250 and 1500 V. The source was mounted on a hinge arrangement to allow cleaning or milling of an optic and sputtering a target without breaking vacuum.

Deposition Rate Monitor. An Inficon mod. XTM quartz crystal rate monitor was used. Rate, accumulated thickness, and elapsed time were displayed.

Chemical Purities. Chemicals used were of optical purity and were purchased from either CERAC, Inc. or II-VI, Inc. These included ThF_4 , MgF_2 , ZnS , and ZnSe , which were 99.99%, 99.9%, 99.99% and 99.999% pure, respectively.

Electron Microscope. A Philips 501B was used to examine substrates. The resolution of the instrument was specified at 90\AA . However, this did not prove to be very useful since the substrates examined were found to have structure smaller than this. This was used to examine substrates for relatively gross defects.

Spectrophotometers. A Cary 17 was used for uv and visible characterization of optical transmission; a Perkin-Elmer 580B was used for the IR.

Thermal Deposition Sources. To deposit dielectric material thermally, Balzers secondary, indirect sources were used. They were constructed either of Mo or Ta.

During thermal deposition of dielectric materials, the chamber vacuum was in the low 10^{-6} Torr range. Prior to deposition the substrate was ion beam cleaned with the source adjusted to produce a beam of 300-400eV ions. The substrate was rotated during cleaning. Total exposure time was usually 1/2 to 2 minutes, depending on the substrate material. Care was taken to avoid sufficient exposure to produce surface roughening due to ion milling. After cleaning, a shutter covered the substrate while the deposition source was heated. The substrate was uncovered when a rate of 50 to 100Å/sec was reached. For ZnS and MgF₂ the substrate was heated to 150°C and 250°C, respectively; during deposition of ZnSe and ThF₄, the substrate was heated to 100°C. During deposition the substrate was rotated.

During ion beam sputter deposition of dielectric materials the substrate was either kept at ambient temperature (~ 50°C) or was heated to 120°C to 250°C, depending upon the dielectric being deposited. During deposition of Cu the substrate temperature was at ambient (~ 50°C). The substrate was not rotated during the deposition.

When substrates (coated or uncoated) were ion beam milled, shutters were used to allow only a portion of the substrate to be milled at a time. In this manner three areas of the substrate could be milled with different ion beam doses, and one area of the substrate could be left unmilled to be used as a reference. It was felt that this was a good procedure for obtaining overlap in sample-to-sample data. Also it made economical use of samples. Not considering the processing time for the milling, the cost of some samples was over \$100. Over 40 samples were milled in this manner. From these, 25 were examined for surface roughness using Total Integrated Scattering at the Naval Weapon Center, China Lake, Ca. Each of the four areas was examined at approximately 10 points for light scattering. The cost per sample for this analysis was approximately \$110. Other measurements include scanning electron microscope, interferometry and optical transmission.

The Twyman-Green interferometer was constructed from optics that were flat to within approximately $\lambda_{\text{vis}}/20$. The output from a He-Ne laser operating at 6328Å was passed through a spatial filter and collimated. One leg of the interferometer included a 1 1/2" thick window on the vacuum feedthru collar that allowed the laser output to enter the deposition chamber. The two legs encountered five or six optical surfaces each, depending upon the application. The quality of the optics used was sufficient to produce a fairly straight fringe pattern ($\lambda/4$). Also, a lens was used to image the optic being examined onto the plane containing the fringe pattern. This pattern was photographed using a polaroid camera and thus provided a record of the figure of an optic being examined. This arrangement was used extensively in recording the figure of an optic prior to coating or milling and also to determine the amount of milling that had been done. Figure 2(a) shows the fringe pattern obtained with good optics throughout the system; Figures 2(b) and (c) show the typical patterns obtained from one optic that has been milled as described above. Three regions have been milled different amounts, and one region has been unmilled.

Ion beam current density was measured using a homemade Faraday probe which was biased at approximately -30V. Knowing the probe area allowed the measured probe current to be related to beam current density. The ion beam was characterized for several combinations of beam current and voltage.

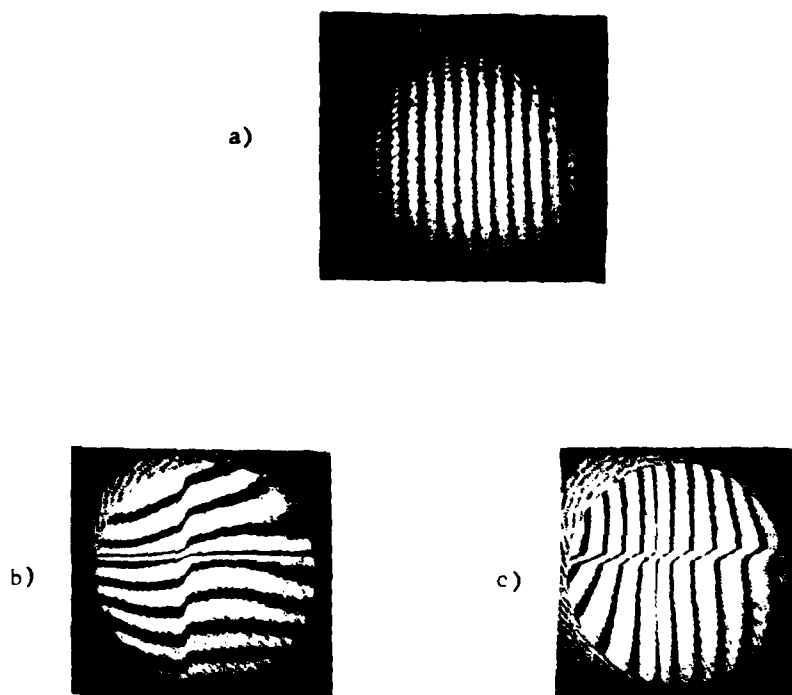


Figure 2. Photographs of interference pattern produced using a Twyman-Green interferometer with one leg in the vacuum deposition chamber with (a) flat optics used throughout in order to test the system, and (b) one optic in the deposition chamber having been milled, showing typical data. Note that the optic was milled different amounts in three regions, with a fourth region left unmilled to be used as a reference.

3.0 RESULTS AND DISCUSSION

The interferometer incorporated into the deposition chamber proved to be very useful, and few problems arose during its use. The next three sections describe work in which the interferometer was used.

3.1 Selective Deposition and Milling to Improve the Figure of an Optic.

Figures 3 and 4 illustrate the results obtained when using a single shutter to selectively control ZnS deposition and milling of an optical surface. Similar results were obtained milling uncoated metal substrates. As shown in Figure 3(b), the surface was intentionally made to have a step of approximately 1500Å in the thickness of the ZnS coating. After this, the shutter and the optic were adjusted for milling position. With a total beam current of 60 mA and voltage of 500V, the optic was milled for approximately 3 minutes. Figure 3(c) shows the result. It can be seen that the surface was brought to a figure close to the original condition shown in Figure 3(a) within approximately $\lambda/8$. The sequence of Figure 4 shows a case where the technique was not entirely successful. In this case the optic and the shutter were not properly aligned during period of milling.

It should be emphasized that these results are from use of a simple, one-dimensionally rotatable shutter. In a more realistic situation a combination of shutters might be used, with some possibly being stepper motor controlled in several directions. Also, in a realistic situation the figure for an optic will not change in such an abrupt manner as it was made to do here. The figure might change by some fraction of a wavelength across the entire optic. In this sense, the situation here is an extreme case. More elaborate measures might allow control of surface figure to a small fraction of a wavelength.

This demonstration was performed in situ without breaking vacuum. This is important for two reasons. Economically this is desirable because the optic can be coated, examined, corrected, and recoated in a short period of time. This is to be compared to a process in which the optic is removed from a deposition chamber, mounted for examination, replaced in the deposition chamber and recoated. The process is also very advantageous from a technical viewpoint. When a coating is interrupted by exposure to atmosphere, the coating performance

- a) Uniform Surface
(5000 Å ZnS on Al)



- b) Selectively Mill 1500 Å Step



- c) Repaired Surface

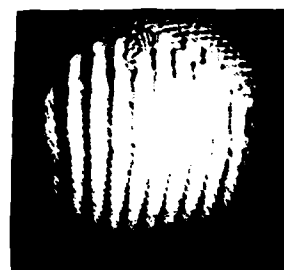
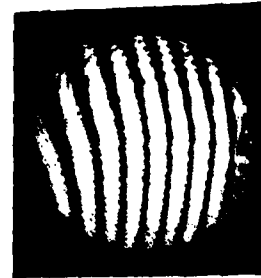
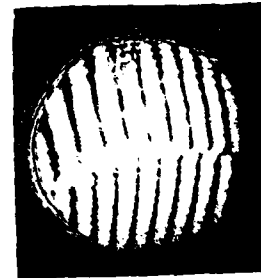


Figure 3. Demonstration of selectively milling an optic to introduce a 1500 Å step and the repair of the optic by selectively milling the opposite side. Note that the repaired surface, part (c), has a figure the same as the original optic, part (a), to within $\sim \lambda/8$.

- a) Uniform Surface
(5000 Å ZnS on Al)



- b) Selectively Deposit ZnS to
produce 1500 Å Step



- c) Partially Repaired Surface



Figure 4. Demonstration of selectively depositing material on an optic to introduce a 1500 Å step and the partial repair to the optic by selectively milling the same side.

is seriously degraded. This is the case when either a single layer is built up with an intermediate exposure to atmosphere or when a multiple layer dielectric stack is being deposited. There is an interface formed by the residual gas atoms trapped between film material. Quality of optical performance is drastically reduced when this occurs.

The time required to correct the figure is directly dependent on the ion beam conditions (current density and voltage) and the sputter yield of the material that is being milled. Table 3 summarizes the sputter rate information derived from the materials milled in this work. This is discussed below.

3.2 Effect of Ion Beam Milling on Surface Roughness and Optical Transmission of Substrate and Dielectric Coating Materials.

3.2.1 Optical Substrate Materials

Figures 5, 6, 7, and 8 illustrate the results of ion beam milling Cu, Mo, Si, and various glass-like materials. The surface roughness determined by Total Integrated Scattering measurements is shown plotted versus milling depth, with milling depth expressed in units of fringes for ($\lambda=6328\text{\AA}$). Thus a milling depth of .5 fringe represents approximately 1500\AA milled from the optic.

It can be seen that Cu does not increase in surface roughness in a very predictable manner for milling more than $1/4$ fringe, if that much. This corresponds to a change of roughly 800\AA . For milling more than $1/4$ fringe, the roughness increases drastically. The exception is the Cu #4 sample. Prior to milling, this sample had a 5000\AA thick layer of Cu ion beam sputter deposited on the surface to be milled. It can be seen that the unmilled region of the sample is approximately 50 to 70% as rough as the unmilled regions of the other Cu samples. Also, the roughness increases more slowly and in a more predictable manner than the roughness of the other Cu samples, to a milling depth of approximately 1.5 fringes. This corresponds to approximately 4700\AA , which is just less than the Cu film thickness.

The increase in roughness for milling depth greater than $\sim 1000\text{\AA}$ might be attributed to the substrate crystal structure becoming apparent. The crystal

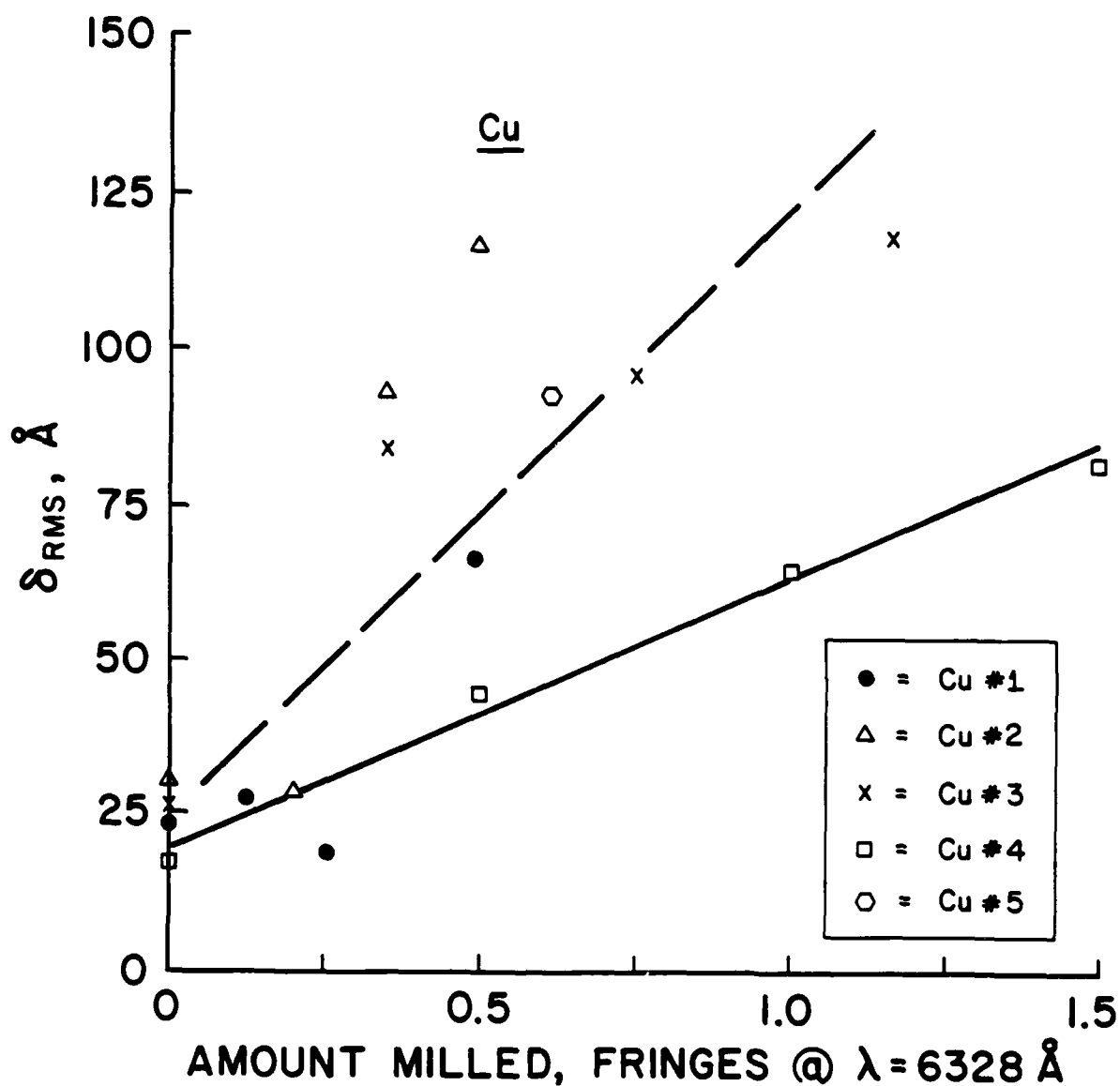


Figure 5. Surface roughness, δ_{RMS} , resulting from ion beam milling Cu substrates, versus milling depth. Note that milling 1 fringe @ 6328 Å corresponds to approximately 3200 Å being removed. The dashed line corresponds to samples 1, 2, 3 and 5; the solid line is for sample #4.

orientations in the polycrystalline substrate are irregular, and this causes the ion impingement angle at the various crystals to be irregular. Also, the sputter yields of materials generally depend on the impingement angle.^{13,14} The various crystal faces are milled different amounts, and this preferential milling produces a rough surface. The behavior shown by the Cu #4 sample deserves more investigation. This is discussed more in the next section.

From Figures 6 and 7 it can be seen that Mo and Si samples can be milled in a predictable manner, with surface roughness increasing only slightly for milling less than 3/4 fringe. Silicon is particularly attractive, with an increase in RMS roughness of approximately 5Å⁰ resulting from milling 1 fringe. It seems reasonable to explain the increase in roughness in terms of the preferential milling mentioned above.

Although examining glass-like materials was not specifically part of the requirements of this effort, this was done because of the widespread use of these materials. From Figure 8 it can be seen that dynasil and 7940 quartz (commercial quartz) increase in roughness with ion milling. This is an increase of less than 100%, which amounts to approximately 10Å⁰ for a total milling depth of approximately 1 1/2 fringe. Although this is a fairly small increase on an absolute basis, it is not clear why there is an increase. This would not be expected because of the amorphous structure of the two materials. The BK7 class samples did not display a noticeable, regular increase in roughness with milling, except possibly for large amounts of milling (>1 1/2 fringe). The scatter in the data shown in the figure could be a result of measurement uncertainty. Here, too, the increase is small on an absolute basis, being approximately 5Å⁰ for 1 1/2 fringe milling.

Similarly, electroless Ni deposited on polished Al substrates was examined. This also was not part of the requirements of this effort. It was examined because of the popularity of the material for use in diamond turned optics and in other optics applications. Figure 9 shows the variation in surface roughness with milling. Very little increase (if any) is observed, and the increase shown could be within the measurement error. The electroless material most likely has very fine grain structure. Only one sample was examined because of costs explained, and care should be taken in drawing too general conclusions from this.

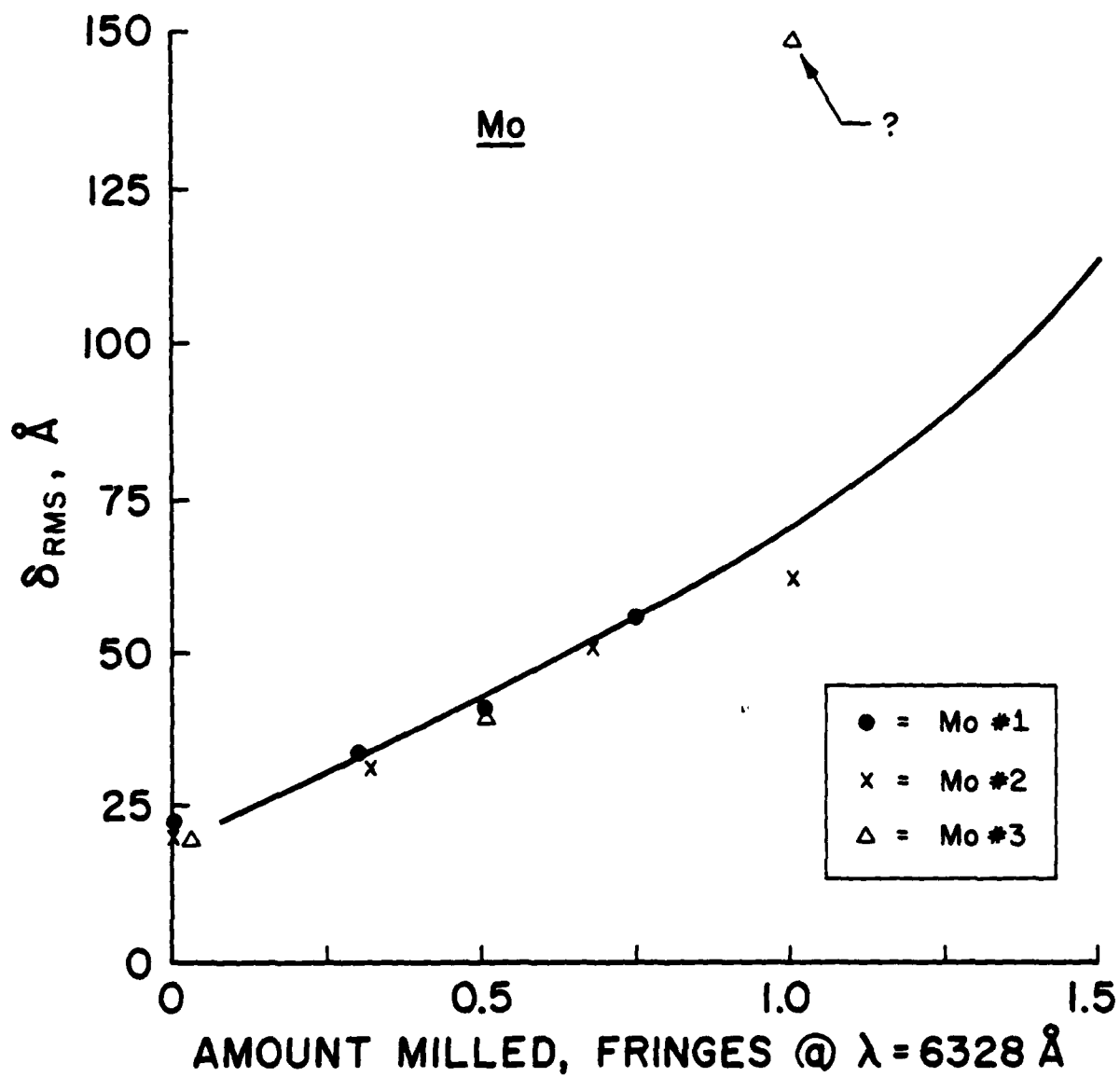


Figure 6. Surface roughness, δ_{RMS} , resulting from ion beam milling Mo substrates, versus milling depth. Note that milling 1 fringe @ 6328 \AA corresponds to approximately 3200 \AA being removed.

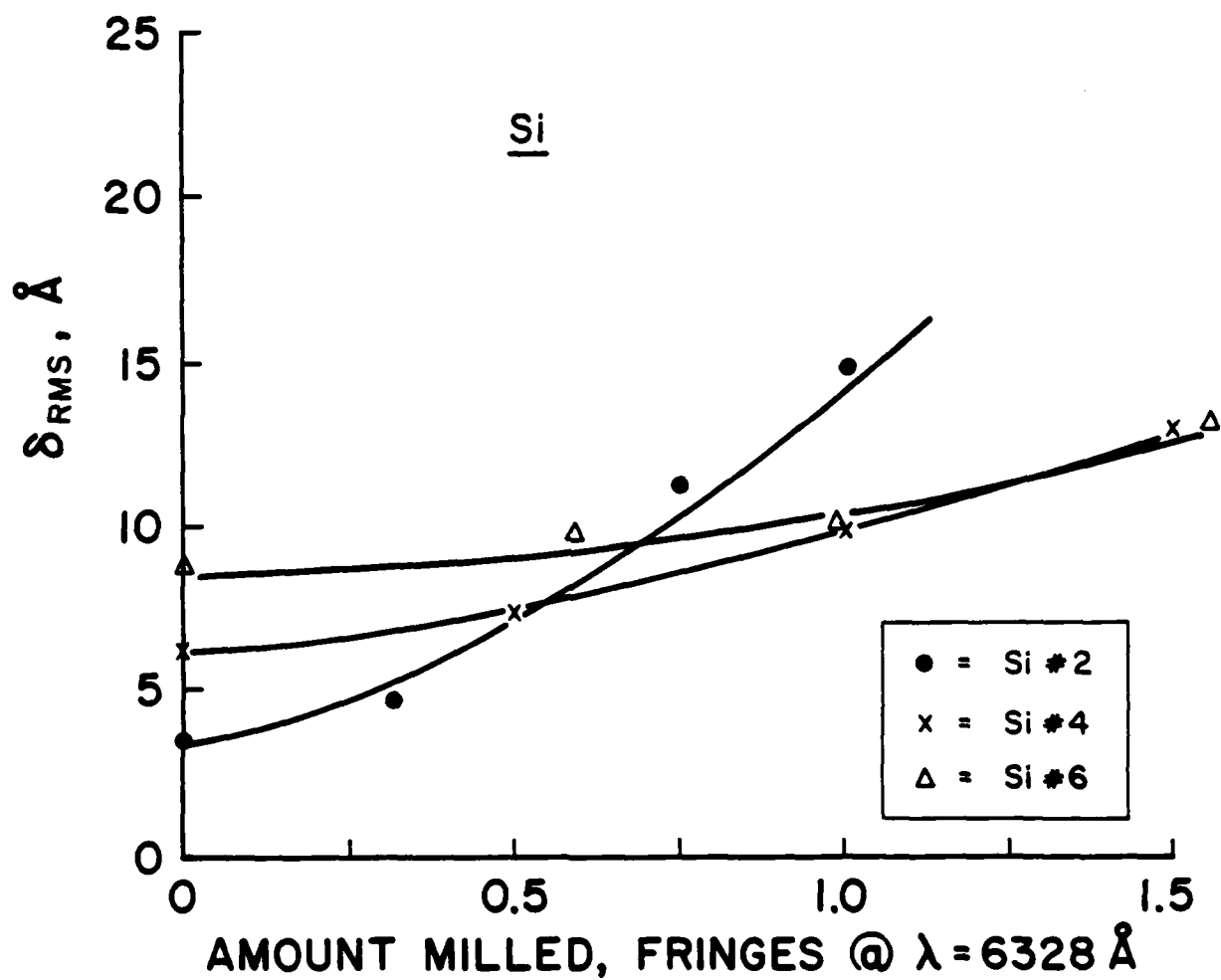


Figure 7. Surface roughness, δ_{RMS} , resulting from ion beam milling Si substrates, versus milling depth. Note that milling 1 fringe @ 6328 \AA corresponds to approximately 3200 \AA being removed.

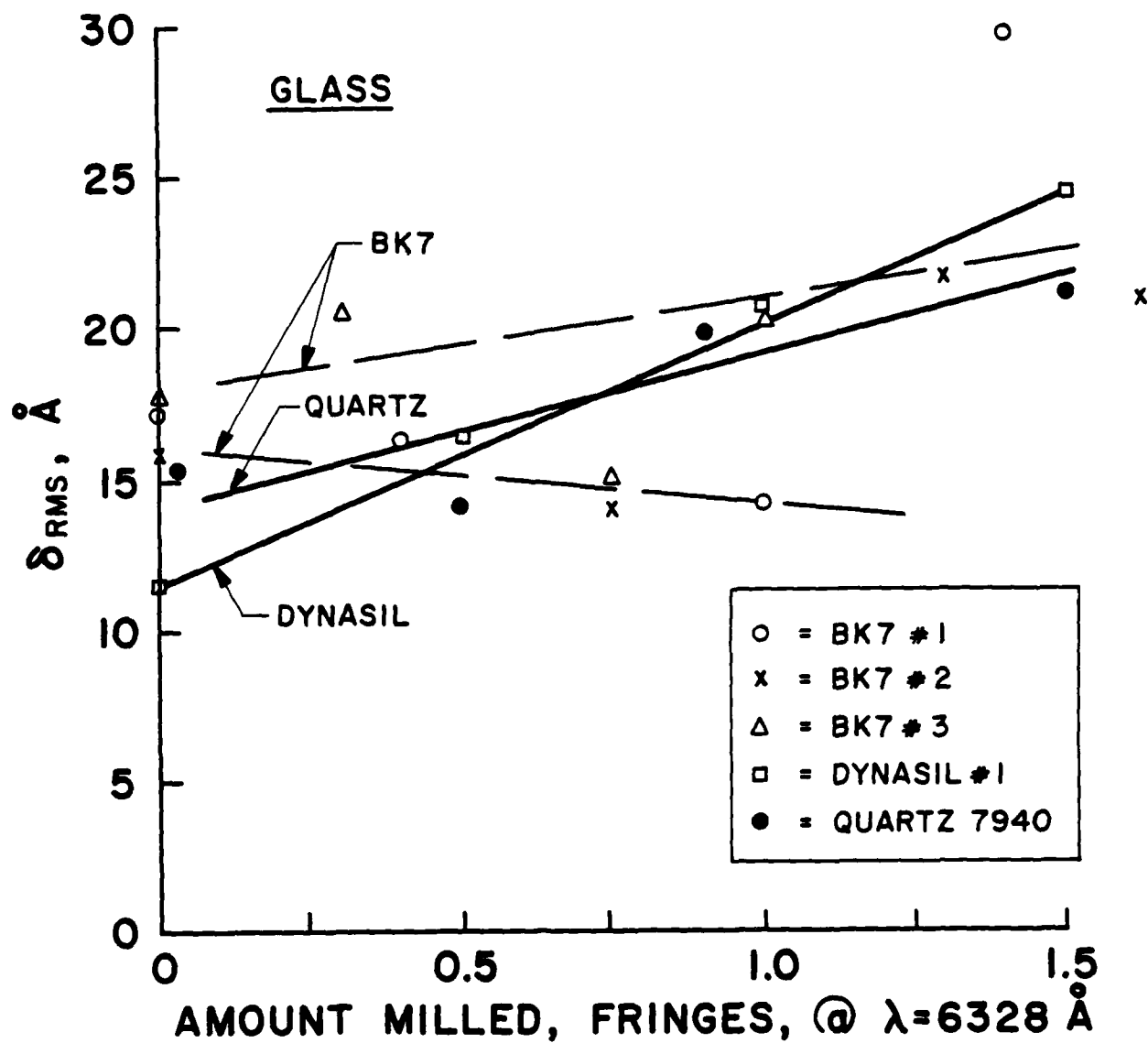


Figure 8. Surface roughness, δ_{RMS} , resulting from ion beam milling different glass-like materials substrates, versus milling depth. Note that milling 1 fringe @ 6328\AA corresponds to approximately 3200\AA being removed.

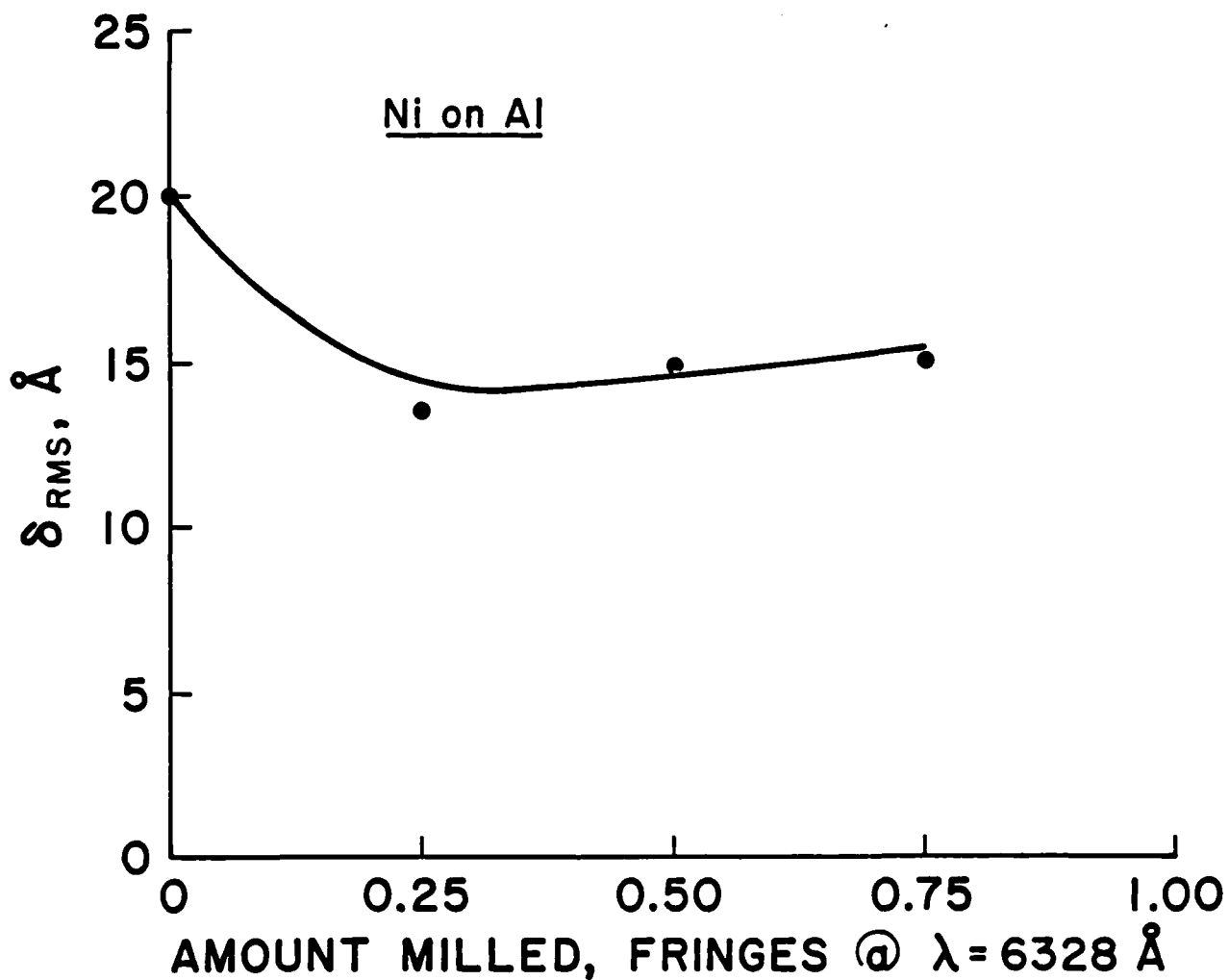


Figure 9. Surface roughness, δ_{RMS} , resulting from ion beam milling electroless Ni on Al substrates, versus milling depth. Note that milling 1 fringe @ 6328\AA corresponds to approximately 3200\AA being removed. Care should be taken in generalizing these results since only one sample was examined.

3.2.2 Dielectric Coating Materials

Figures 10, 11, 12, and 13 illustrate the results of milling ZnS, ZnSe, ThF₄ and MgF₂, respectively. The deposition conditions were described in Section 2. Substrate material used in most cases was Si because of the low RMS roughness observed previously. It can be seen that ZnS and ZnSe display very little increase in roughness, 5-10Å for milling up to 1½ fringe. Similarly, ThF₄ and MgF₂ display little increase in roughness, 10Å, for milling up to 1 fringe; milling more than this causes a pronounced increase.

The deposition rate and the substrate temperature most likely have an effect on the roughness that can be observed after milling. Lower substrate temperature and higher deposition rate, for example, would tend to reduce the surface mobility of atoms. This in turn would cause the crystallite size of the dielectric material to decrease. Also, contamination and residual gasses can influence the crystallite size considerably. If the crystallite size were smaller than that in the films examined in this work, the surface roughness would probably be less than that shown in the figures.

Ion milling the surface of the film might be expected to change the surface stoichiometry of the film and thus affect the optical transmission. Films of ThF₄ and ZnS were characterized for optical transmission before and after being milled by 1 1/2 fringes. No detectable difference could be observed in transmission. The ion beam milling most likely affects the stoichiometry of the ThF₄ film (see Section 3.4) and might affect that of the ZnS film. However, since the surface of the film is being continuously sputtered away, it is doubtful that any change in composition would exist deeper than a few atomic layers in the film. A more sensitive technique (e.g., Auger analysis) is needed to detect an effect this small.

In two cases the film crazed during milling, once when a ZnS film was milled and once when ThF₄ was milled. This was most likely due to energy deposited in the optic by the ion beam. Conditions of the beam were extreme when this occurred, with beam current of 60 mA and beam voltage of 1500V. The temperature of the optic was monitored when BK7 glass was milled with a beam of the same conditions. The temperature exceeded 250°C after 8 minutes milling.

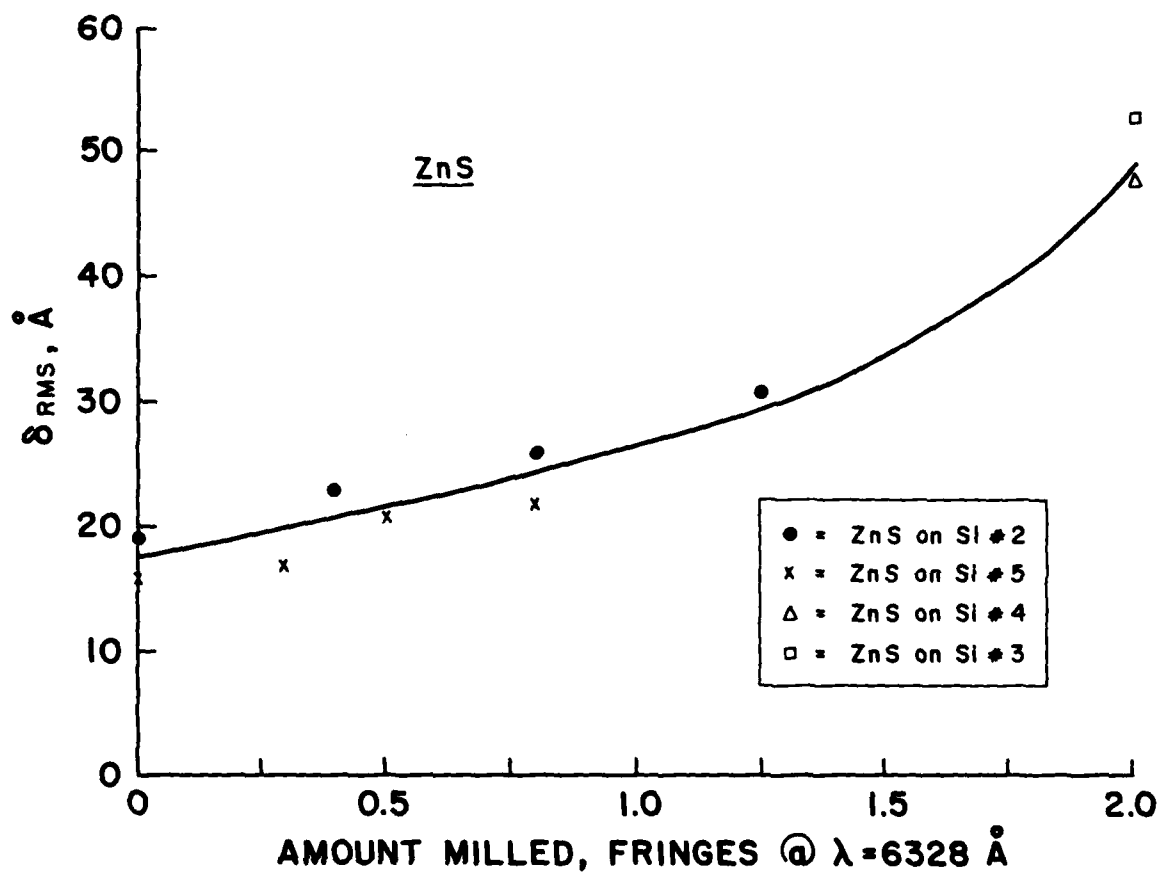


Figure 10. Surface roughness, δ_{RMS} , resulting from ion beam milling ZnS substrates, versus milling depth. Note that milling 1 fringe @ 6328 Å corresponds to approximately 3200 Å being removed.



Figure 11. Surface roughness, δ_{RMS} , resulting from ion beam milling ZnSe substrates, versus milling depth. Note that milling 1 fringe @ 6328\AA corresponds to approximately 3200\AA being removed. Note that care should be taken in generalizing these results since only one sample was examined.

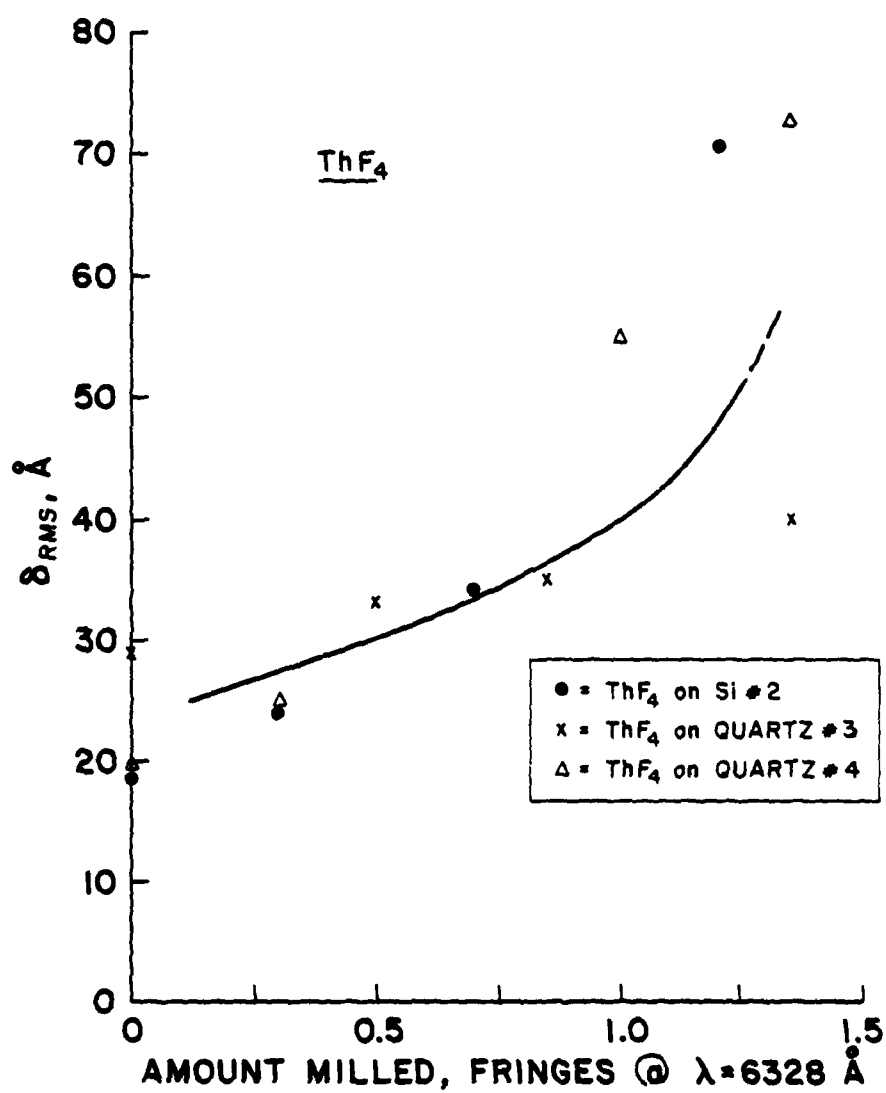


Figure 12. Surface roughness, δ_{RMS} , resulting from ion beam milling MgF_4 substrates, versus milling depth. Note that milling 1 fringe @ 6328 \AA corresponds to approximately 3200 \AA being removed.

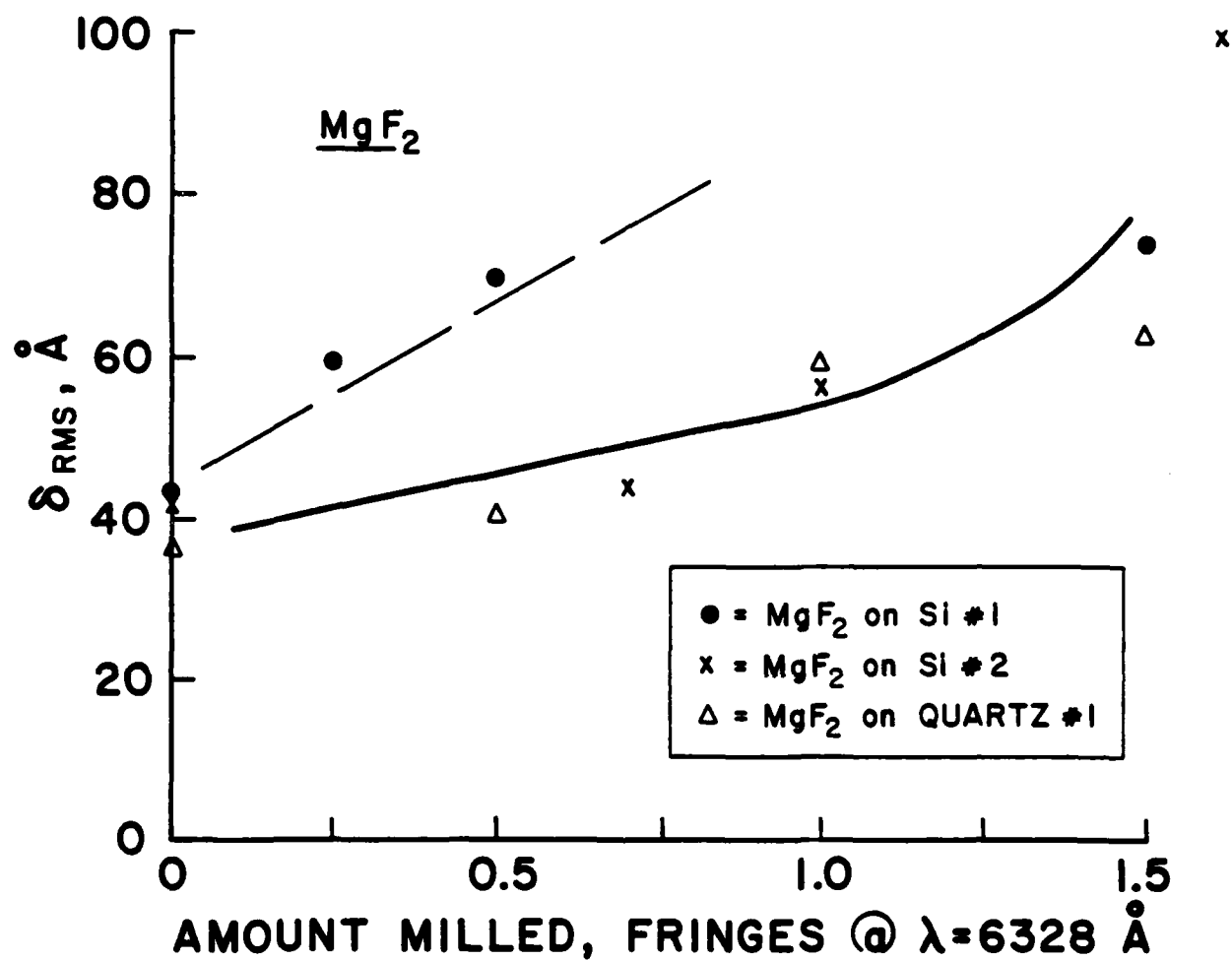


Figure 13. Surface roughness, δ_{RMS} , resulting from ion beam milling MgF₂ substrates, versus milling depth. Note that milling 1 fringe @ 6328 Å corresponds to approximately 3200 Å being removed.

Within 2 minutes after the beam was turned off, the temperature was approximately 90°C. Better thermal sinking would have improved the situation.

3.2.3 Surface Roughness Dependence on Ion Beam Milling Parameters

Most of the samples investigated in this work were milled with the ion beams incident at the optical surface at an angle of 30° from the surface. The beam current was usually 30 or 60 mA, and beam voltage ranged between 500 and 1500 V.

One might expect the roughness of a milled optic to depend to some extent on the angle the optic makes with the ion beam. This could be expected from geometrical arguments, where, for example, an extended portion of the surface might shadow a portion of the surface behind it. This would prevent portions from being milled. Similar arguments have been made concerning deposition of thin film material at oblique angles of incidence.²⁰ Indeed, some work in Reference 8 involved milling with an ion beam nearly parallel to the optical surface. However, there is a limit to the practicality of this technique.

Table 2(a) summarizes the results of milling Cu samples at different angles. The substrates were not rotated during milling. For Cu #5 there is little difference in roughness seen in milling 0.7 fringe with the beam making angles of 30° and 90° with the optical surface. Similarly, little difference is seen in milling 0.5 fringe at angles of 60° and 90°. The values of roughness of the two samples might have been more nearly the same if the same amounts had been milled. Thus, within this range of 30° to 90°, there is little effect of angle observed.

Beam voltage was varied in milling samples of Si and ZnS. Table 2(b) summarizes the results. The results shown for ZnS indicate the roughness increases by 30 to 50% when using a higher beam voltage. The 2 fringe, 500 V data is consistent with the data of Figure 8. Data from Si sample was not what was expected. From Table 2(b) it can be seen that milling 0.7 fringe yields a rougher surface than milling 1 fringe. The 7.8 Å roughness for the surface milled 1 fringe using a beam voltage of 1500 V is consistent with the data of Figure 6. Data from this Si sample for the region milled 0.7 fringe is thus questionable.

	δ_{RMS}			
	Unmilled	30°	60°	90°
Cu#5	19.8Å	93.Å; 0.7 fringe		65.2Å; 0.5 fringe
Cu#6	27.5Å		76.1Å; 0.5 fringe	65.2Å; 0.5 fringe

(a)

	δ_{RMS}		
	Unmilled	500V	1500V
Si#5	7.3Å	16.1Å; 0.7 fringe	7.8Å; 1 fringe
ZnS on Si#3	15.3Å	53.3Å; 2 fringes	71.2Å; 2 fringes
ZnS on Si#4	14.4Å	48.2Å; 2 fringes	73.2Å; 2 fringes

(b)

Table 2: Effects of ion beam milling on surface roughness for different experimental conditions: (a) variation of ion angle of incidence to the normal from optical surface, and (b) variation of beam voltage.

3.3 Sputter Rates of Materials

Feasibility of applying ion milling techniques is, in part, dependent on the time required to mill a material. This depends on a number of parameters, including the sputter yield for the particular ion-target combination and the beam conditions. The sputter rates observed for the materials examined in this work are summarized in Table 3. In the table, the beam current I refers to the total current from the source, while the current density J was measured at the substrate. Most data is for the beam making a 30° angle with the substrate. Note that several materials were sputtered under different beam conditions. The sputter rate increases significantly with beam voltage. From the trend indicated, the sputter rate for Mo might be expected to increase by a factor of 2 or 3 with a beam voltage of 1500 V. The last two columns are useful when determining the economics of the process. Because the sputter rate scales linearly with beam current density, the data in the "fringes/min" column was divided by that of the " J , mA/cm²" column. The resulting information is shown in the last column and is of a more general nature.

Note that most of these rates reflect a sputter yield that is consistent with values observed previously. For example, for Cu milled with a 500 V beam, the yield $Y(500)$ atoms/ion is expressed in terms of the sputter rate R as

$$R = [Y(500)] \frac{J}{e} \frac{\text{Atoms}}{\text{cm}^2\text{-sec}} \quad (4)$$

where e is electronic charge. Assuming a crystal ionic radius of $.96 \text{ \AA}$ for Cu for approximating the volume V of a Cu atom in the substrate²¹, this becomes

$$\begin{aligned} R' &= (V R) \times 10^{-16} \frac{\text{\AA}}{\text{sec}} \\ &= [Y(500)] \frac{J}{e} V \times 10^{-16} \frac{\text{\AA}}{\text{sec}}, \end{aligned} \quad (5)$$

where R' is the rate shown in Table 3. Solving for $Y(500)$ yields a value of 3.5 atoms/ion, which is comparable to the values of 2.0 and 2.4 reported²². The difference could be due to measurement of J or calculation of V .

Material Milled	Beam Conditions			Sputter Rate		
	I, mA	J, mA/cm ²	V	°/sec	fringes/min	fringes-cm ² /mA-min
Cu	60	0.53	500	4.3	0.083	0.15
Cu	60	0.83	1500	9.0	0.17	0.20
Si	60	0.53	500	5.3	0.10	0.19
Si	30	0.44	1500	26.	0.50	1.1
Mo	60	0.53	500	2.9	0.056	0.10
ZnS	60	0.53	500	8.7	0.17	0.31
ZnS	60	0.53	1500	35.	0.67	0.80
ZnSe	60	0.53	500	13.	0.25	0.47
ThF ₄	60	0.83	1500	15.	0.28	0.33
MgF ₂	60	0.73	1000	5.8	0.11	0.15
Dynasil	60	0.73	1000	7.3	0.14	0.20
Quartz 7940	60	0.73	1000	10.	0.20	0.27
BK7	60	0.53	500	2.9	0.056	0.11
BK7	60	0.83	1500	19.2	0.37	0.45

Table 3: Summary of ion milling rates of the samples investigated.

3.4 Effect of Ion Beam Sputter Deposition to Reduce Surface Roughness

Figure 5 and Table 4 illustrate the reduction in surface roughness produced by ion beam sputtered Cu deposition. The unmilled region of the Cu #4 sample is approximately 50 to 70% as rough as the unmilled regions of the Cu #1, #2 and #3 samples. As explained previously, the Cu #4 sample was ion beam sputter coated with approximately 5000 Å of Cu prior to any milling. Note also that the milled regions of Cu #4 are less rough than the corresponding regions of the other Cu samples.

As a second investigation of the effectiveness of sputter deposition, the Cu #1, #2, and #3 samples were reexamined. Those samples were originally milled and analyzed as summarized in Figure 5. They were then coated with Cu using ion beam sputtering. The surface roughness of the samples before and after coating are compared in Table 4. It can be seen that in most cases the surface roughness after coating is less than that before coating. Even for as little as 1000 Å of deposited Cu, there is a significant reduction in surface roughness. These two results indicate a trend in which ion beam sputter deposition has a tendency to smooth rough surfaces.

Two things should be noted. First, it has been shown²³ using Talystep measurements that metallic films deposited using standard resistive-heated sources preserve the substrate surface topography to a resolution of several (2-4) Angstroms for film thickness up to 1000-2000 Å. Typical temperature of resistive-heated sources is 1200-1500°C; thus particles from such a source arrive at the optical substrate with an energy of ~ 0.1 eV. It appears then that the surface smoothing effect observed in this work is a result of the high energy of sputtered particles and not simply a masking of the surface irregularities by the deposited film.

The second point concerns the fact that several of the ratios of Table 4 are greater than unity, indicating an increase in roughness from the film deposition process. One possible explanation for this is that the optic surface became contaminated (dust, etc.) after the initial measurement of surface roughness. Between this time and the second measurement of roughness, a time of over two months, the optics were handled, packed and unpacked several times.

Sample: Cu#1, 1000Å Deposited

Amount Milled, fringes @ $\lambda = 6328\text{\AA}$

	0	.13	.25	.40
$\frac{\sigma_{\text{RMS}}(\text{After})}{\sigma_{\text{RMS}}(\text{Before})}$	$\frac{16.5}{27.2} = .61$	$\frac{19.9}{19.1} = 1.04$	$\frac{28.9}{29.4} = .98$	$\frac{48.1}{69.5} = .69$

Sample: Cu#2, 4000Å Deposited

Amount Milled, fringes @ $\lambda = 6328\text{\AA}$

	0	.20	.35	.50
$\frac{\sigma_{\text{RMS}}(\text{After})}{\sigma_{\text{RMS}}(\text{Before})}$	$\frac{21.3}{32.5} = .66$	$\frac{34.6}{29.5} = 1.17$	$\frac{71.0}{94.1} = .75$	$\frac{100}{118} = .85$

Sample: Cu#3, 2000Å Deposited

Amount Milled, fringe @ $\lambda = 6328\text{\AA}$

	0	.35	.75	1.1
$\frac{\sigma_{\text{RMS}}(\text{After})}{\sigma_{\text{RMS}}(\text{Before})}$	$\frac{23.5}{25.7} = .91$	$\frac{67.6}{84.5} = .80$	$\frac{108}{96.8} = 1.12$	$\frac{65.9}{118} = .56$

Table 4: Effect of Ion Beam Deposited Cu Films on Surface
Roughness of Ion Beam Milled/Roughened Surfaces.

An explanation of the smoothing behavior observed is not straightforward. The surface roughness of a deposited film is determined by the statistical process of nucleation and growth, and these are described in terms of a diffusion process of condensate adatoms. Kinetic theory of gases may be applied in some cases. An important parameter which determines film growth is the surface mobility of an adatom. Deposition conditions that strongly influence mobility include adatom temperature (kinetic energy), impingement angle of adatoms, deposition rate, substrate material, substrate temperature and substrate roughness. The term "mobility" cannot be defined quantitatively since it is influenced by so many physical parameters. In spite of this, the pronounced effect of adatom kinetic energy on mobility has been well established²⁴. Some treatments relate aspects of the diffusion process to adatom temperature by an $e^{-Q/kT}$ dependence, where Q is an activation energy or the energy barrier between absorption sites. Here T is the equilibrium temperature of the adatom and the substrate. Sputtered particles, with energies of 1-10eV are not initially in thermal equilibrium with the substrate when they become adatoms. In this case the exponential dependence is not as simple as above.

For low temperature deposition where atomic mobility is small, the surface roughness, or average deviation, σ from the average film thickness t is governed by Poisson statistics and can be expressed as²⁵

$$\sigma = \sqrt{t} \quad (6)$$

At higher adatom temperature (or substrate temperature), surface mobility becomes more effective. Mobility is also greater for more oblique angles of adatom impingement. Thus, as illustrated in Figure 14, the condensation might occur preferentially at surface concavities and thus tend to smooth the surface. Other investigators have found that when depositing Fe films using an evaporation source, the film roughness decreases with increasing temperature of the evaporation source. Similarly, the roughness increases markedly when films are deposited in the presence of ambient gases, presumably a result of rapid thermalization of the adatom and reduction of surface mobility.

Two other possible explanations for the surface smoothing include the forward sputtering of Cu material by arriving Cu atoms. Peaks would be sputtered and valleys would be filled somewhat. Another possibility is that the sputtered Cu layer has smaller grain structure than the substrate.

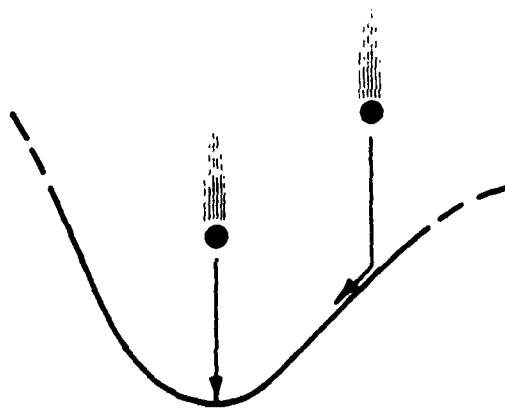


Figure 14. Illustration of how energetic atoms, which become adatoms with high surface mobility, might tend to reduce micro-roughness of a surface.

3.5 Ion Beam Deposition of Dielectric Coating Materials

In this investigation the dielectric materials most investigated were ZnS, MgF₂, and ThF₄. This was because of the general popularity of these materials for visible and IR applications.

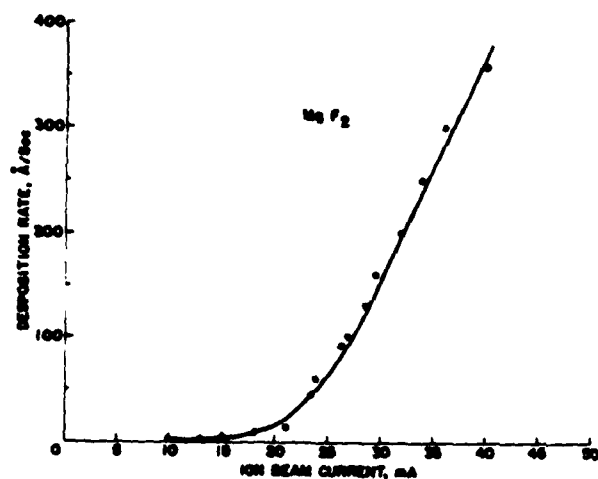
3.5.1 Sputter-Thermal Deposition Technique

There are two drawbacks to sputter deposition of optical materials. One is the relatively low deposition rate obtained for most materials. Also, related to this is the nonuniform deposition achieved. This results from placing the optical substrate close to the sputter target to help increase deposition rate.

We have demonstrated a technique using ion beams to incorporate the advantages of sputter deposition that also achieves high deposition rates to overcome the disadvantage mentioned. This technique was successful with ZnS and MgF₂ but not with ThF₄. The deposition process first included pre-cleaning by ion beam bombardment of the substrate. The ion source was then directed onto the sputter target and used to sputter the target material onto the optical substrate. During this stage of deposition, the total ion beam current was low (< 20mA). The sputter deposition rate increased linearly with ion beam current and was relatively low for a current less than approximately 20mA. See Figure 15. In this case the beam acceleration voltage was 1500V. Increasing the beam current past 20mA in the case of MgF₂ and past 35mA in the case of ZnS caused the deposition rate to increase drastically. We attribute this increase in deposition rate to thermal effects resulting from target heating by the ion beam. If this is the case, then the majority of particles arriving at the substrate have thermal kinetic energy. Note that the rates indicated in Figure 15 correspond to the geometry of our arrangement, with approximately 6" between the ion source and the sputter target as well as between the sputter target and the optical substrate.

This same technique was employed using internal funding of Optic Electronic, Corp. to investigate other materials (Ge and Ge-As-Se glass). See Reference 15 for details.

(a)



(b)

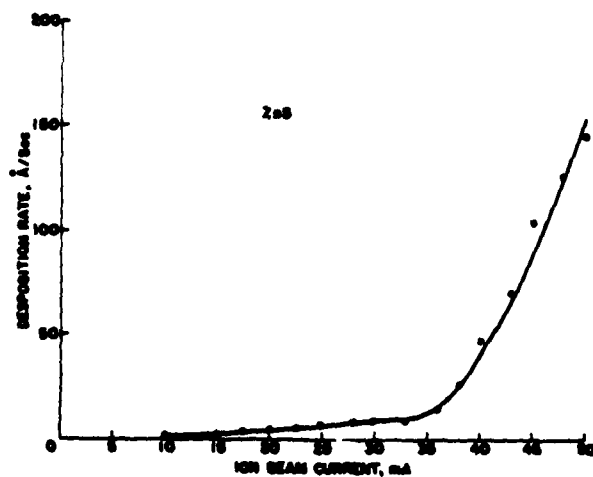


Figure 15. Deposition rate observed (for the particular geometry employed) versus ion beam current for ion beam deposited (a) ZnS and (b) MgF_2 , illustrating sputter-thermal deposition of dielectric material.

Unfortunately, this technique was not successful with ThF_4 . When the ion source was operated with a beam output of 80mA and 1500V, the deposition rate at the optic was less than 1 Å/sec. This was prohibitively slow to allow deposition of several $\lambda/4$ layers at 10μ ; approximately 5 hours would be required for each ThF_4 layer. The lifetime of the ion source cathode is 4 to 6 hours operating at this level. The ThF_4 target was supported by thin Al to minimize conductive cooling. Ar, Ne, CF_4 , and O_2 were used in attempts to increase this rate as well as to investigate the optical properties of sputtered ThF_4 .

3.5.2 Optical Properties of Ion Beam Sputtered ZnS and ThF_4

A Perkin-Elmer 580B spectrophotometer was used to characterize the coating performance. More sensitive calorimetry measurements should be performed for coatings intended for high energy laser applications.

Figure 16(a) shows the spectrophotometer trace of an Ar-sputtered ZnS film on Ge substrate at approximately 120°C . The film was $\lambda/4$ at approximately 11μ . The deposition rate was 10 Å/sec. Also shown is the transmission characteristic of bare Ge. No absorption can be detected from the figure. Other coatings of different thicknesses yielded similar results.

Figure 16(b) and (c) indicate the results of sputtering a ThF_4 target. The substrate for both cases was Ge at a temperature of 120°C . Also shown is the characteristic of uncoated Ge. The first time the ThF_4 target was exposed to the ion beam was in producing the coating of Figure 16(b). As can be seen, there is considerable absorption ($\sim 6\%$) in the 10μ region. After sputtering the target for several hours and exposing it to atmosphere, the target material changed color from a beige to a dark gray. The sputtered film produced from this "aged" target had the transmission characteristic illustrated in Figure 16(c). It is uncertain from this if there is significant absorption at 10μ . The film thickness was $\lambda/4$ at approximately 1μ .

The behavior illustrated in Figures 16(b) and (c) has not been explained. However, it is likely due to oxygen reacting with the ThF_4 that has been exposed to the ion beam. The ThF_4 bond is easily broken by the Ar-ion, leaving the target material deficient in F. It is likely that O_2 from water

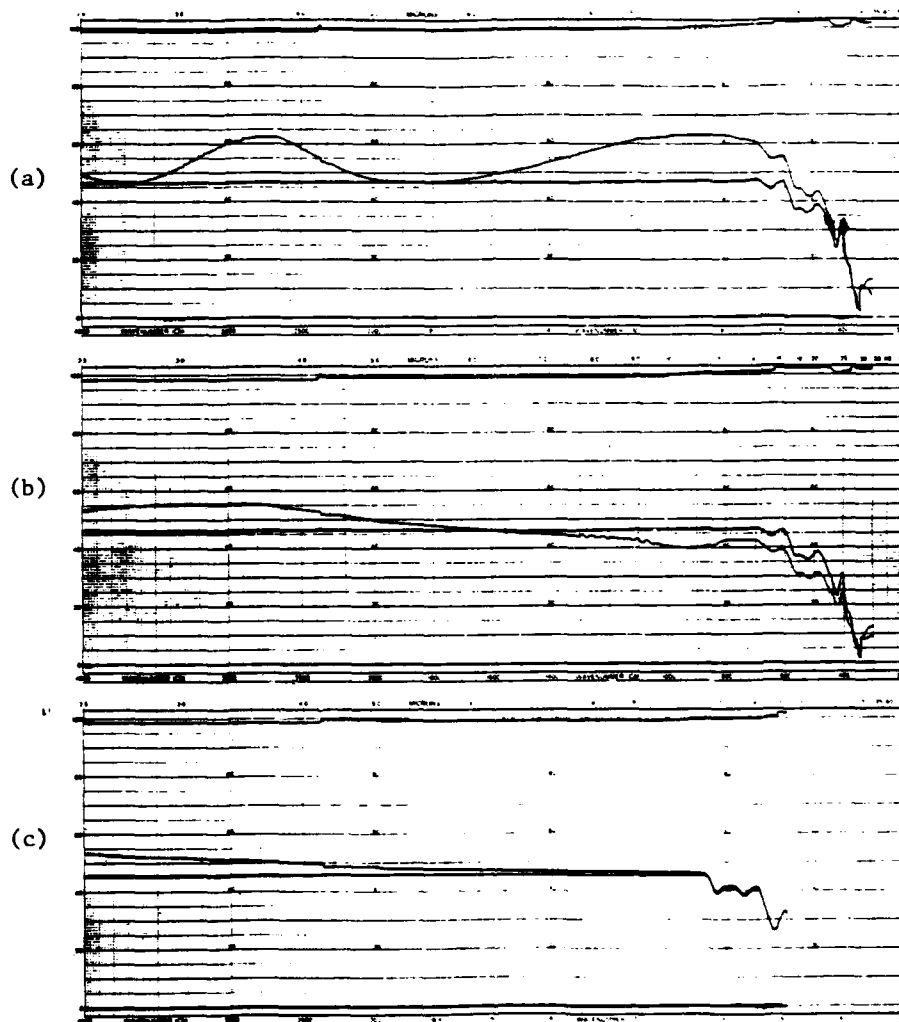


Figure 16. Spectrophotometer scans of ion beam deposited films of (a) ZnS, (b) ThF₄, and (c) ThF₄. See text for explanation of difference in conditions for depositing (b) and (c).

vapor or other residual gas (base pressure $\sim 2 \times 10^{-6}$ Torr) or from exposure to atmosphere might cause formation of Th-O-F combinations. These compounds (ThOF_2 and Th(OH)F_3) are fairly absorbtive at 10μ , with β values of 3 to 10cm^{-1} . This would cause at most an absorption of 1% for the films investigated here, which is not accurately detectable using the spectrophotometer.

In summary, ion beam sputter or sputter-thermal deposition of ZnS appears to be good techniques, while for ThF_4 it appears questionable. More sensitive analysis techniques, such as calorimetry are needed.

3.5.3 Future Possible Applications of Ion Beams to Thin Film Coating

The deposition of ThF_4 in this work using ion beam sputtering was not satisfactory. However, this gave rise to ideas of other possible uses of ion beams during deposition of thin film materials in general.

The ion beam might be directed onto the optical substrate during the deposition of thin film material. The material might be dielectric or metallic, and it could be generated from an independant source, such as a resistively heated boat, e-beam source, etc. In this way, fast deposition might be achieved along with potential advantages resulting from ion beam bombardment. Momentum exchange at the optical surface between energetic ions from the ion source and low energy thin film material might produce energetic atoms of thin film material on the surface of the optic. This would possibly lead to films with properties similar to sputter-deposited films, such as superior adhesion and increased packing density. This technique has been used by other investigators^{26,27} to vary the intrinsic stress of evaporated Cr and Ge. Preliminary investigations by the author and W. C. Herrmann, Jr. have shown the technique reduces the intrinsic stress of evaporated MgF_2 and $\text{ThF}_4/\text{AlF}_3$ multilayer coatings. This technique might be used to vary the columnar structure of thin films and reducing the total void volume in a film. Biasing a substrate during r-f sputtering has been used to change the structure of dielectric films. Similar results could likely be obtained using the ion beam technique described, but with more control available of ion energy, density and incidence angle using an ion beam.

4.0 SUMMARY

The accomplishments of this effort can be summarized as follows:

- (1) Cu does not appear satisfactory for being ion milled to improve surface figure.
- (2) Ion beam sputter deposition of Cu onto Cu substrates tends to reduce microroughness of the substrates.
- (3) The other materials examined -- Mo, Si, glasses, electroless Ni, ZnS, ZnSe, MgF_2 , and ThF_4 -- can be milled in a controlled manner. The amount that can be milled from the optic without severe increase in roughness depends upon the application. However, in general the increase in roughness for milling less than 0.5 fringe is less than the initial surface roughness of the optic.
- (4) The value of the interferometer for in-vacuum monitoring of optic surface figure has been demonstrated to:
 - A. Selectively deposit material on an optic and selectively ion beam mill an optical surface; repair a nonuniform optical surface.
 - B. Repeated deposit/mill/deposit optical material without breaking vacuum.
- (5) Ion beam sputter deposition of ZnS appears to produce films of good optical quality; deposition of ThF_4 using ion beam sputtering produces films of questionable absorbance. A hybrid technique for deposition of ZnS has been demonstrated, that incorporates advantages of sputter deposition and thermal deposition. The sputter yield of ThF_4 is too low in the present geometry to make the process viable. More detailed investigations of these films are needed.

References

1. H. E. Bennett and D. K. Burge, "Multilayer Thickness Uniformities Required to Meet Wavefront Error Tolerances in Laser Mirrors", presented at the 12th Annual Symposium on Optical Materials for High Power Lasers, Boulder, Co., Sept. 30 - Oct. 1, 1980. See also H.E. Bennett, in Laser Induced Damage in Optical Materials: 1976, A. H. Guenther and A. H. Glass eds. (NBS Spec. Publ. 462; 1976), pp 11-21.
2. J. B. Schroeder, H. D. Dieselman, and J. W. Douglas, "Technical Feasibility of Figuring Optical Surfaces by Ion Polishing", Appl. Optics, 10, 295 (1971).
3. C. B. Hogge, R. R. Butts, and M. Burkakoff, Air Force Weapons Laboratory Technical Report (AFWL-TR-73-131), pp 105-122 (1973).
4. Personal correspondence, Mr. Cy Denny, SPAWR Optical Research Corp.
5. F. E. Johnson, M. E. Curcio, D. C. Smith and L. E. Lockett, "Diamond Turning Produces Precise Infrared Optics", Laser Focus, pp 33-36, July (1981).
6. A. L. Bloom and D. Fischer, J. Opt. Soc. Am. 69 p. 1438 (abstract only) 1979.
7. R. A. Hoffman, W. J. Lange, J. G. Gowan, C. J. Miglionico, "Ion Polishing as a Surface Preparation for Dielectric Coating of Diamond-Turned Optics", to be published.
8. R. A. Hoffman, W. J. Lange, and W. J. Choyke, "Ion Polishing of Copper: Some Observations", Appl. Opt. 14, 1803 (1975).
9. R. A. House, J. R. Bettis, and H. G. Guenther, "Efficacy of Ion Polishing Optical Surfaces," Appl. Optics 16, 1486 (1977).
10. See also A. B. Meinel, S. Bashkin, and D. A. Loomis, "Controlled Figuring of Optical Surfaces by Energetic Ionic Beams", Appl. Optics 4, 1674 (1965). J. B. Schroeder, H. D. Dieselman, and J. W. Douglas, "Technical Feasibility of Figuring Optical Surfaces by Ion Polishing", Appl. Optics 10, 295 (1971).
11. G. R. Thompson, Jr., "Ion Beam Coating: A New Deposition Method", Solid State Tech., p. 73, December 1978.
12. D. M. Mattox, "Fundamentals of Ion Plating", J. Vac. Sci. Techrol. 10, 47 (1973); see also G. Gautherin and Chr. Weissmantel, "Some Trends in Preparing Film Structures by Ion Beam Methods", Thin Solid Films 50, 135 (1978).
13. G. K. Wehner, "Sputtering by Ion Bombardment", Handbook of Thin Film Technology, ed. by L. I. Maissel and R. Glang, McGraw-Hill (1970).
14. C. G. Wejsenfeld, A. Hoogendorn, and N. Koedam, "Sputtering of Polycrystalline Metals by Inert Gas Ions of Low Energy", Physical 27, 763 (1961).

15. W. C. Herrmann, Jr. and J. R. McNeil, "Ion Beam Deposited Ge-Se-As Glass for Applications in the 1 μ to 16 μ Wavelength Region", presented at the 12th Annual Symposium on Optical Materials for High Power Lasers, Boulder, Co., Sept. 30 - Oct. 1, 1980.
16. R. L. Gaver and H. J. Sequin, "High Quality Sputtered Multilayer Coatings for Infrared Laser Applications", Rev. Sci. Instr., 41, 427 (1970).
17. J. L. Vossen, RCA Rev., 32, 289 (1971).
18. D. B. Fraser and H. D. Cook, J. Electrochem Soc., 119, 1368 (1972).
19. K. L. Chopra, Thin Film Phenomena, p. 183, McGraw-Hill, 1969.
20. Ibid., p. 177.
21. CRC Handbook of Chemistry and Physics, ed. by R. C. Weast and M. J. Astle, p. F152, The Chemical Rubber Publishing Company, 1969.
22. J. L. Vossen, in Thin Film Processes, ed. by J. L. Vossen and Werner Kern, p. 15, Academic Press, 1978.
23. J. M. Bennett, personal correspondence.
24. K. L. Chopra, op. cit., pp. 165-199.
25. Ibid., p. 185.
26. E. H. Hirsch and I. K. Varga, Thin Solid Films, 52 p. 445, (1978).
27. D. W. Hoffman and M. R. Gaerttner, "Modification of Evaporated Chromium by Concurrent Ion Bombardment", J. Vac. Sci. Technol. 17 (1980).

ATE
LMED
8